Article

Influence of Precursor Mixtures on the Laser Chemical Vapor Deposition of TiC Fibers

Kendall J. Mitchell and Gregory B. Thompson *

Department of Metallurgical & Materials Engineering, University of Alabama, P.O. Box 870202, Tuscaloosa, AL 35487, USA; kmitchell18@crimson.ua.edu
* Correspondence: gthomps@ua.edu

Abstract: In this study, the hyperbaric (2 bar) laser chemical vapor deposition of TiC fibers grown under various percent pressures of hydrogen and ratios of ethylene and titanium tetrachloride (2:1 or 1:1) are reported. In the hydrogen-rich (85%) condition, sequential fiber depositions became stunted as a result of a loss of hydrogen, which served as a reducing agent for the metal halide as hydrogen evolved with the hydrocarbon gas in the reaction zone because of the Le Chatelier principle. For the hydrogen-lean (25%) condition, the intrinsic fiber growth rate was invariant, but gas phase nucleation resulted in the hydrocarbon forming carbon soot in the chamber which subsequently deposited and coated on the fibers. In the hydrogen-balanced composition (50%), the 2:1 precursor ratio resulted in inconsistent intrinsic growth rates which ranged from approximately 30 μm/s to 44 μm/s. However, for the hydrogen-balanced (50%) 1:1 condition, the intrinsic growth rate variation was reduced to approximately 12 μm/s. The differences in fiber uniformity, composition, and structure under these process conditions are discussed in terms of hydrogen's ability to serve as a reducing agent, a fluid to transport heat from the deposition zone, and alter the structure of the fiber through thermophoresis.

Keywords: LCVD; UHTCs; TiC fibers

1. Introduction

Extreme environments, such as those found in hypersonic flight, requires materials which have high melting temperatures, high fracture toughness, and high thermal shock resistance. Ultra-high temperature ceramics (UHTCs) can meet some of those demands as they have melting points over 3000 °C, but, as is characteristic of ceramics, they have a low thermal shock resistance and low fracture toughness [1,2]. Conventionally, these mechanical property issues are overcome using carbon and silicon carbide-based fiber reinforcements to increase shock resistance, fracture toughness, and overall material strength for UHTCs in a composite form [3]. However, these types of fibers have a lower temperature resiliency. For example, silicon carbide begins to oxidize and ablate in aerospace applications above 1600 °C [4,5]. Consequently, there is an identified need for the development of new fibers which can endure ever increasing temperatures. Titanium carbide (TiC), which is a UHTC, would be such a material and could act as a strengthening fiber for UHTC ceramic-matrix-composites [1,6].

TiC fibers can be traditionally synthesized by electrospinning [7–9] or by coating TiC onto a carbon fiber through chemical vapor deposition (CVD) [10] or by a molten salt synthesis route [11]. In this work, we explore the direct formation of TiC fibers through laser chemical vapor deposition (LCVD), where no such carbon fiber substrate is required. Comparable to hot wall CVD, LCVD utilizes a pyrolytic reaction of precursor gases to deposit the material under the focal point of the laser which serves as the primary heat source [12,13]. By retracting the laser focal point, deposition continues and a free-standing fiber grows directly from the vapor-to-solid phase transformation. This process can be scaled-up by the employment of multiple lasers and/or a beam splitter to enable several

such beams to facilitate simultaneous growth. A benefit of LCVD over electrospinning synthesis or conventional CVD is the accuracy of deposition, which allows for possibilities to make complex 3D structures such as rods or helixes [14,15]. Additional benefits include the potential for stoichiometric phase control for TiC through gas mixture [16] as well as high deposition rates to control the microstructure [17,18].

To date, there are a rather limited number of reports concerning LCVD TiC fibers [19,20]. In the work by Westburg et al. [20], the LCVD TiC deposition was grown as singular lines across a substrate, referred to as 'strings', in a hypobaric condition. The precursor gases flowed through a hot wall CVD chamber and a laser directed the deposition on the substrate. In more recent work, Fronk et al. [19] reported the hyperbaric LCVD of TiC to deposit free-standing TiC fibers under various laser powers. While hydrogen, ethylene, and titanium tetrachloride were the gas mixtures in both of these reports, neither paper provided a thorough investigation into the gas chemistry mixtures on growth. The gas chemistry, particularly hydrogen, is especially important as its ratio with the carbon gas source is reported to dramatically influence growth rates, deposition morphologies, and microstructures in carbide-based CVD processes [21,22]. In this paper, specific variations in gas composition are addressed in a hyperbaric batched LCVD process for TiC fibers.

2. Materials and Methods

The precursors used to deposit TiC included hydrogen (H_2), ethylene (C_2H_4), and liquid titanium chloride ($TiCl_4$), with respective purities of 99.999%, 99.9%, and 99.9%. The $TiCl_4$ was contained in a pressure vessel directly connected to the reaction chamber and heated to 250 °C to bring it into the gas phase. The H_2 and C_2H_4 vessels were kept at ambient lab temperatures. Each gas was then flowed into a 400 cm^3 semi-spherical cube vessel that was warmed to 200 °C with heat tape and insulation placed around the stainless steel chamber to ensure that the $TiCl_4$ remained in the gas phase during deposition. After the vessel was evacuated using a cryogenic absorption pump that housed zeolite traps along with baking soda that neutralize any condensate HCl (post-deposition), the precursor gases were then flowed into the chamber to a total pressure of 2 bar. Table 1 summarizes the percent pressures of the precursor used during each fiber growth. The concentration of H_2 and the ratio of C_2H_4:$TiCl_4$ were chosen to expand upon conditions from previous work for a hydrogen-rich, hydrogen-balanced, and hydrogen-lean environment [19,20].

**Table 1.** The percent pressure of gases used during each growth.

Percent Pressures of Gases during Each Growth Composition		
	H_2	C_2H_4	$TiCl_4$
Hydrogen-rich (2:1)	85	10	5
Hydrogen-balanced (2:1)	50	33	17
Hydrogen-lean (2:1)	25	50	25
Hydrogen-balanced (1:1)	50	25	25

Using these gases, the ideal stoichiometric reaction for TiC deposition is as follows:

$$2TiCl_4(g) + C_2H_4(g) + 2H_2(g) \rightarrow 2TiC(s) + 8HCl(g) \tag{1}$$

As commented on in the introduction, hydrogen is critical to the reaction as it serves as a reducing agent for $TiCl_4$ and binds excess chlorine to reduce it as a hazard. A continuous wave, 10 W ytterbium 1064 nm laser with a 100 mm focal length lens shined through a 33.8 mm sapphire viewport onto a 5 mm thick tantalum carbide (Ta_2C) substrate. The substrate had a 0.25 μm diamond polish over the surface to reduce its reflectivity. The laser emission was set to and held at 6.5 W throughout each fiber growth. A camera was positioned normal to the laser viewport through another 33.8 mm diameter sapphire viewport to monitor the fiber growth speed. Once the fiber initiated growth, the laser was retracted at a pre-determined axial growth speed with the determination of which

discussed below. Each fiber was grown to a target of 12 mm in length, when possible. After completing this growth length, the laser was turned off, repositioned back to its initial location, and translated 2 mm in-plane whereupon another fiber was then initiated, and the process was repeated. This was repeated for ten fiber deposits for each condition whenever possible. At the conclusion of the deposition, the vessel had the remaining precursor gases evacuated, the chamber walls were cooled, and the fibers were removed and separated from the substrate. A visual representation of the experimental setup is shown in Figure 1. This experimental set up is similar to a prior LCVD chamber reported by the authors in [23], with the added addition of heating tape and insulation around the deposition chamber to ensure that the chamber temperature exceed the boiling point of the metal halide precursor so that it remained in the gaseous phase.
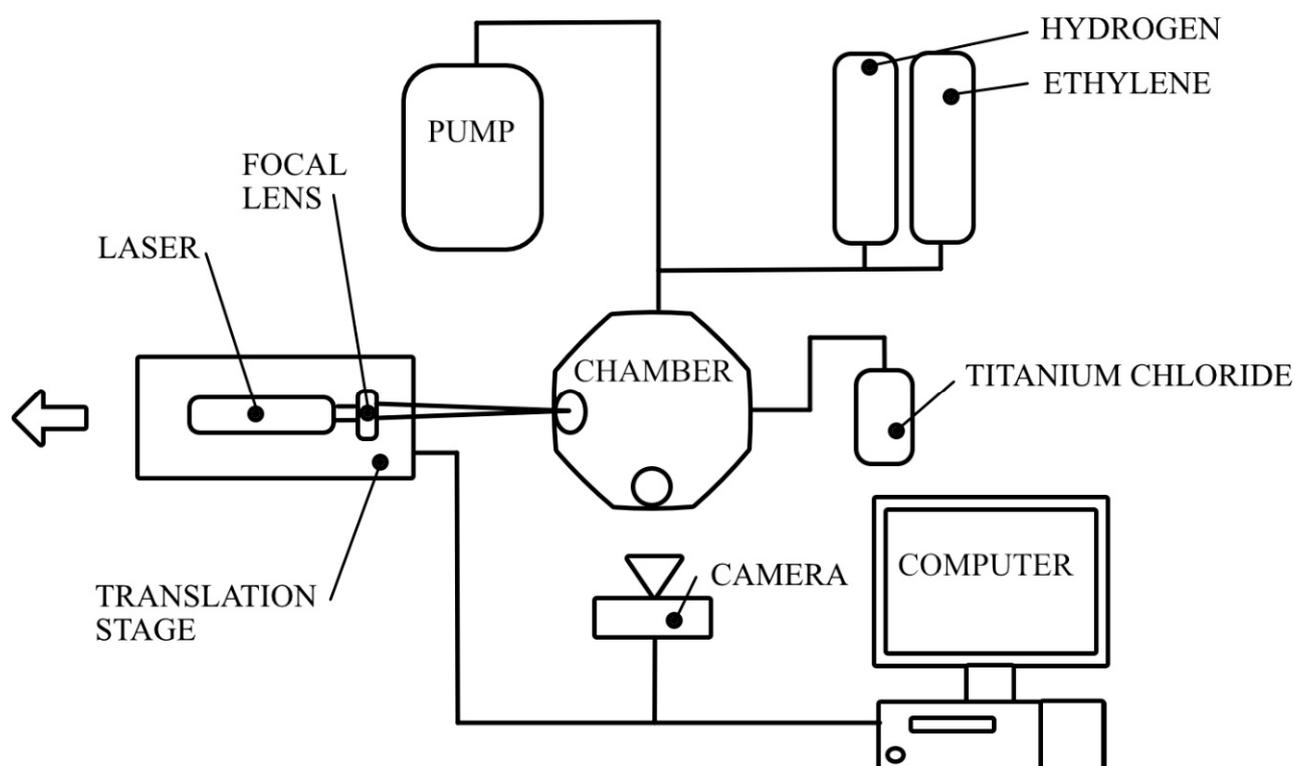

Figure 1. A schematic of the LCVD setup.

To determine the intrinsic growth rate at each gas mixture condition, a fiber was initiated under the laser focal point, but the laser did not translate. Here, the deposit would grow from the focal point where its hot spot was tracked by a video feed until it ceased growing. The stage was shifted by 1 mm and this procedure was performed again $10\times$ to achieve an average measurement of the intrinsic growth rate via a calibrated pixel-to-length calculation. For the hydrogen-rich condition, the speed was set to 3 µm/s; for the hydrogen-balance condition, it was set to 30 µm/s; and for the hydrogen-lean condition, it was set to 40 µm/s.

The structure of the fibers were characterized by a high intensity Rigaku XtaLAB Synergy-R DW—Single Crystal X-Ray diffractometer. The XRD source was Mo and individual fibers were epoxied to a glass mounting rod and secured onto the goniometer. The morphology of the fibers was captured using a Keyence VHX-7000N digital microscope as well as by scanning electron microscopy (SEM) using a Thermo Fisher Apreo instrument (Waltham, MA, USA). For the SEM analysis, the fibers were secured using conductive carbon tape onto a stub and then imaged at 15 keV.
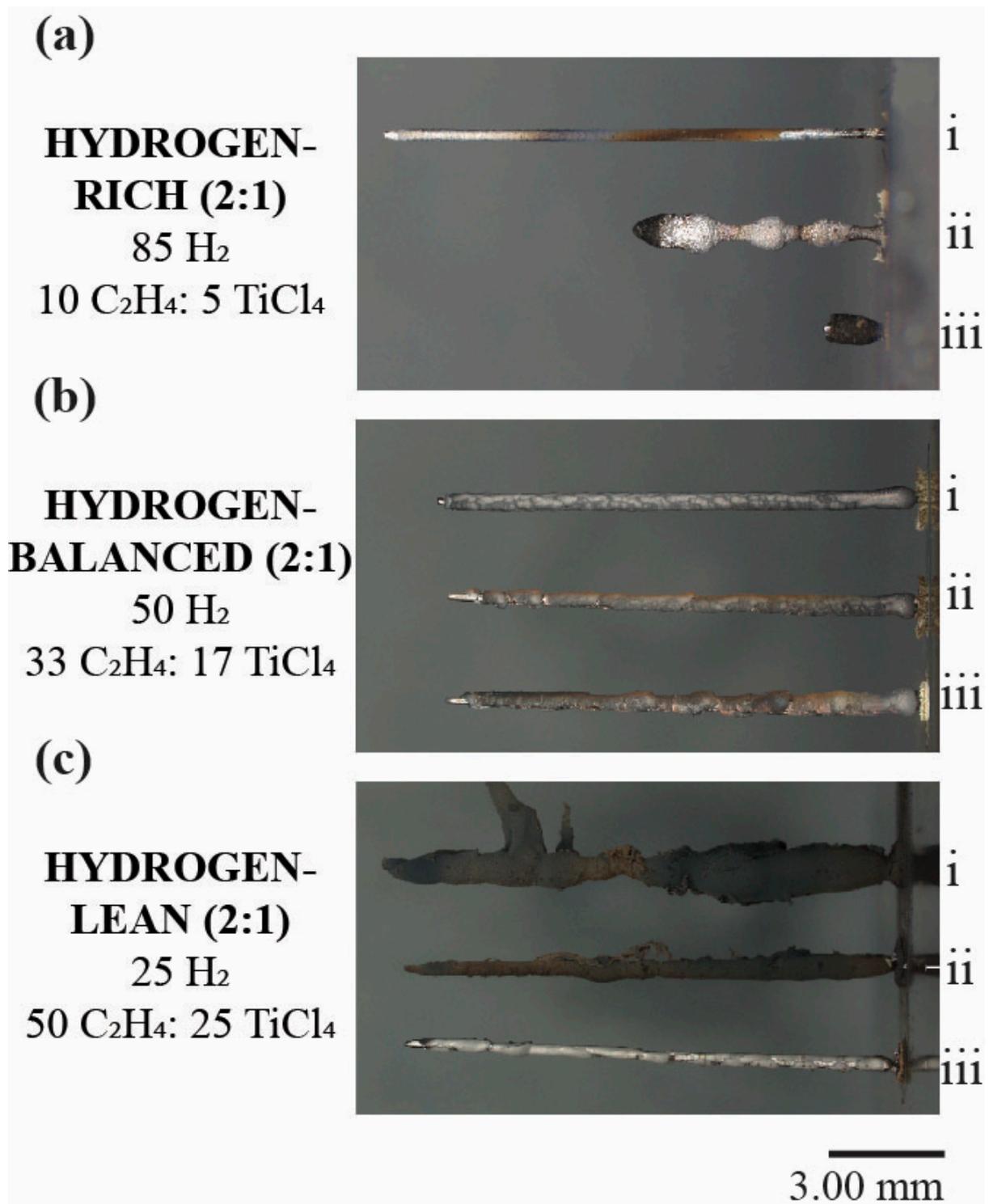
3. Results and Discussion

The standard progression for the TiC fiber growth under the laser focal point are shown in a series of time-lapse images in Figure 2 for the 2 C_2H_4:1 $TiCl_4$ ratio for various hydrogen mixtures. Gaseous convection created by the heat of the reaction was present in each mixture condition, evidenced by the spectral reflection of the beam in the chamber. As can be further gleaned in the time-lapsed images in Figure 2 (at t_2), the hydrogen-rich mixture revealed a significant thermal tail along the fiber length as it deposited. This is contributed to the high thermal conductivity of hydrogen, which ranges from ≈190 to 310 mW/mK over 23 °C to 350 °C; for comparison, air is 26 to 46 mW/mK over the same temperature range. A closer inspection of these time-lapse images, particularly at t_3 for the hydrogen-rich condition, revealed a circumventing dendritic-like deposit at the base around the fiber as seen in Figure 2a. These deposits have been previously determined to be $TiCl_2$ and $TiCl_3$ byproducts, along with carbon soot which nucleates from the high temperature provided by the laser upon initiating the deposition [19,24]. The relatively reduced size of these dendritic deposits for the hydrogen-balanced and lean conditions highlights how the gas mixtures influence, at least, the heat transfer in and around the fiber as it deposits.
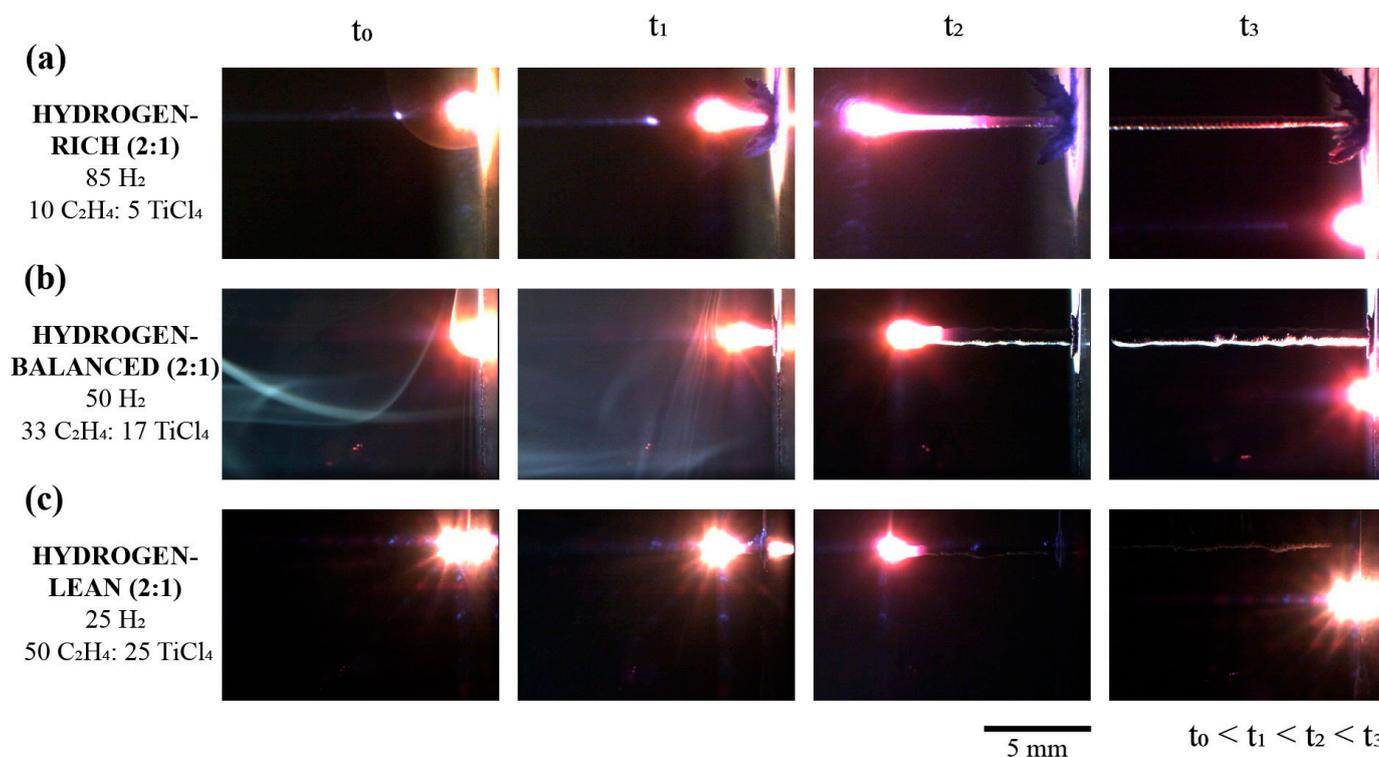
Figure 2. Series of time-lapse images for the 2 C_2H_4:1 $TiCl_4$ mixtures with hydrogen for the TiC fiber growth. (**a**) Hydrogen-rich (**b**) Hydrogen-balance and (**c**) Hydrogen-lean mixtures.

Figure 3 shows a series of digital images for the post-deposited, first three fibers grown under the various hydrogen (2:1) mixtures with their fiber lengths tabulated in Table 2. In the hydrogen-rich (2:1) deposits, the ability to grow each subsequent fiber became ever more difficult evidenced by a decreasing fiber length, as seen in Figure 3a. While the initial fiber, (i), retained a uniform and linear shape, the second fiber, (ii), exhibited a modulated fiber diameter along its length and a termination of growth at approximately half the height of the first fiber. This variation in diameter highlights the difficulty to initiate and maintain a uniform deposition. The third fiber, (iii), which was even shorter than the second deposit, (ii), had its growth stunted at the very early onset of deposition and would not continue to

grow after this height. No other fibers were able to be deposited after this third fiber at this hydrogen-rich concentration.

(a)

HYDROGEN-RICH (2:1)
85 H_2
10 C_2H_4: 5 $TiCl_4$

i
ii
iii

(b)

HYDROGEN-BALANCED (2:1)
50 H_2
33 C_2H_4: 17 $TiCl_4$

i
ii
iii

(c)

HYDROGEN-LEAN (2:1)
25 H_2
50 C_2H_4: 25 $TiCl_4$

i
ii
iii

3.00 mm

Figure 3. Digital images of TiC fibers in the sequence of their subsequential growth sequence of i, ii, and iii, for the first, second, and third deposition for the (**a**) Hydrogen-rich (**b**) Hydrogen-balanced and (**c**) Hydrogen-lean conditions. The numerals i, ii, and iii denote the sequence of the fiber growth with i being the first, ii being the second, and iii being the third.

Table 2. Measurements of fibers taken from Keyence VHX-7000N at 20x. Up to six measurements per diameter per fiber was collected. For the hydrogen-lean condition, the soot was removed prior to measurement to reveal the fiber size.

	Fiber No.	Length (mm)	Average Diameter (mm)	Cross Sectional Area (mm^2)
Hydrogen-rich (2:1)	1	12.93	0.31	0.07
	2	6.56	0.67	0.21
	3	1.47	0.64	0.33
	Average	6.99 ± 4.69	0.49 ± 0.21	0.21 ± 0.32
Hydrogen-balanced (2:1)	1	12.71	0.47	0.18
	2	12.44	0.49	0.19
	3	12.44	0.53	0.23
	Average	12.53 ± 0.13	0.50 ± 0.07	0.20 ± 0.10
Hydrogen-lean (2:1)	1	12.00	0.99	0.80
	2	11.64	0.49	0.21
	3	11.64	0.35	0.10
	Average	11.76 ± 0.17	0.61 ± 0.25	0.37 ± 0.35
Hydrogen-balanced (1:1)	1	12.23	0.63	0.31
	2	12.46	0.74	0.42
	3	12.35	0.71	0.40
	Average	12.37 ± 0.09	0.68 ± 0.05	0.38 ± 0.05

To rationalize the inability to continue to deposit sequential fibers in the hydrogen-rich (2:1) condition, the interaction of hydrogen with the other precursors must be considered. Upon decomposing the ethylene under the laser focus, and in the presence of such a high concentration of hydrogen, ethylene's constituent components will react with hydrogen forming methane, ethane, and propane according to the Le Chatelier principle [25]. In prior work by Cook and Thompson [26,27], these other hydrocarbons are shown to be more difficult to deposit (decompose) by LCVD. With the hydrogen being consumed into these other hydrocarbons, there becomes less hydrogen available to act as a reducing agent for the titanium halide [28]. This in turn impacts the metal decomposition, its growth, and even the metal's reaction with carbon. As seen in the second fiber, Figure 3(a-ii), the instability of the precursor decomposition to be evident by the significant instability to deposit a fiber with a constant diameter. The initiation of the third fiber, Figure 3(a-iii), resulted in minimal deposition, as there is an insufficient availability of hydrogen to act as a reducing agent to promote the deposition reaction given in Equation (1). In addition to these effects, the thermal gradient produced by the laser profile coupled with the high thermal conductivity of hydrogen in the reaction zone led to a variation in the gaseous migration according to its molecular weight, a thermophoresis phenomenon known as the Soret Effect [29,30]. Here, hydrogen occupied the warmer regions of the reaction zone making it more difficult for the other precursors to be co-located with it under the laser focus. This was not an issue in prior work by Westburg et al. [20] because the gas continuously flowed. And, in the hyperbaric condition reported by Fronk et al. [19], where the gas was stagnant as in this work, this paper reported the initial fiber and not the consequences on repeated growth sequences.

In the hydrogen-balanced (2:1) condition, the repeatability of the fiber growth was achieved as evidenced by the similar fiber morphology and consistent fiber height between each subsequent deposit, Figure 3b. In the hydrogen-lean (2:1) condition, the fibers retained a similar height to the hydrogen-balanced (2:1) state, but the subsequent deposited fibers are covered in carbon soot, which was also apparent within the growth chamber and would explain the darker contrast seen in the time-lapse images in Figure 2c. The formation of this errant carbon is attributed to gas-phase nucleation (GPN), which is the homogeneous nucleation of solid particulates directly from the gas phase while outside the focal point of the laser [31]. GPN occurred because a high concentration of ethylene was coupled with sufficient heat generated from the laser within the closed chamber vessel [32]. Once a new

fiber began to deposit, the carbon-soot simply was caught and collected itself onto the previously grown fibers as seen in Figure 3(c-i,ii).

The phase(s) of the fibers, identified by XRD, are shown in the diffractograms plotted in Figure 4. In all cases, multiple diffracted peaks are indexed to TiC. In addition to TiC, for the hydrogen-balanced (2:1) and hydrogen-lean (2:1) conditions, a reflection denoted with an asterisk (*) at approximately 12° and 24° 2Θ was captured and corresponds to graphite. The lack of carbon reflections for the hydrogen-rich (2:1) condition affirmed that if the carbon was not bound to titanium, it likely recombined with the excess hydrogen-rich environment and formed a hydrocarbon gas that became more difficult to dissociate into a carbon deposit, as previously discussed above.
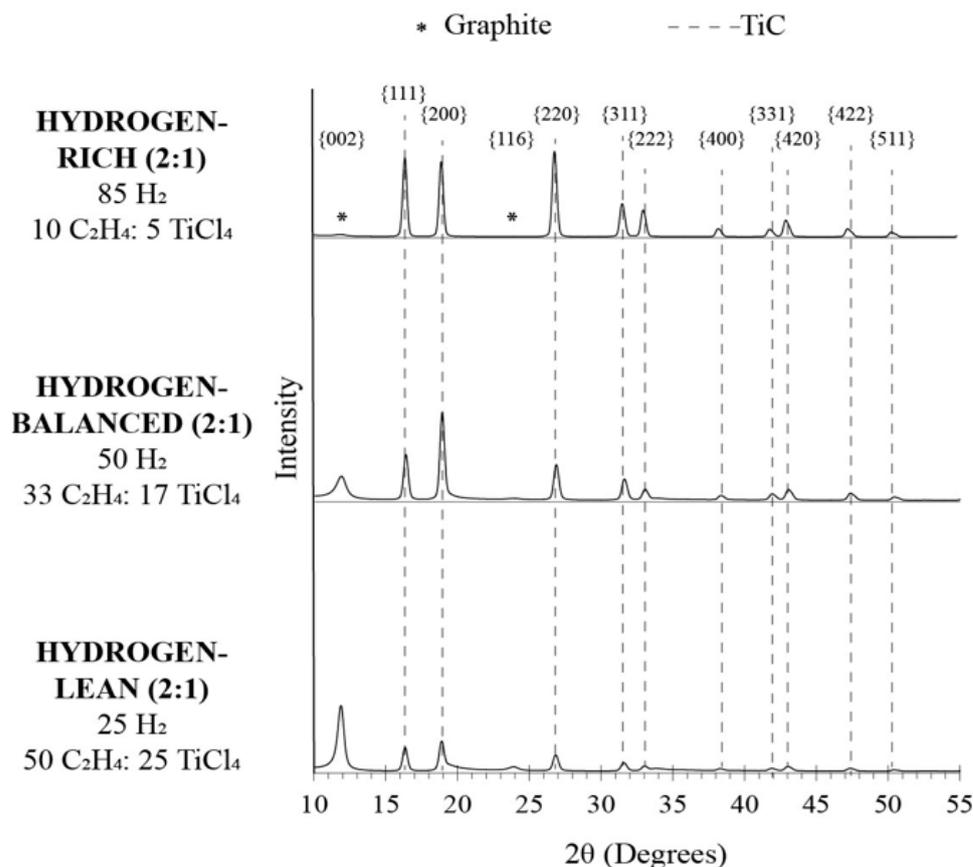
Figure 4. XRD data showing peaks correlating to graphite and TiC peaks.

As seen in Figure 5a, the SEM image for the hydrogen-rich (2:1) condition has a notable hole in the fiber core forming it as a tube. An X-ray Energy Dispersion Spectroscopy (XEDS) line profile across the diameter is plotted alongside this image, where the relative carbon counts are zero in the hole region. While there is a modest Ti X-ray signal in this same region, this contributed to the Ti X-ray signal being collected from the inner core walls of the tube and escaping through the hole. This is further affirmed by the asymmetric count profile of this signal in this region based on the tilt of the fiber to the imaging electron beam shown in the same figure. The lack of carbon X-ray emissions from the same off-axis collection is contributed to its much lower emission energy, as compared to Ti, resulting in it being absorbed and unable to escape through the hole. Note that equivalent hole structure has also been reported by Fronk et al. in TiC fibers [19]. This hole morphology is explained by the aforementioned Soret effect, where the hydrogen gas, at a sufficiently high concentration, excluded the heavier precursor species from the central region under the laser focal point. Consequently, the solid TiC phase was only able to be deposited radially around the gaseous center creating this tube.

(a)

HYDROGEN-
RICH (2:1)

(b)

HYDROGEN-
BALANCED (2:1)

(c)
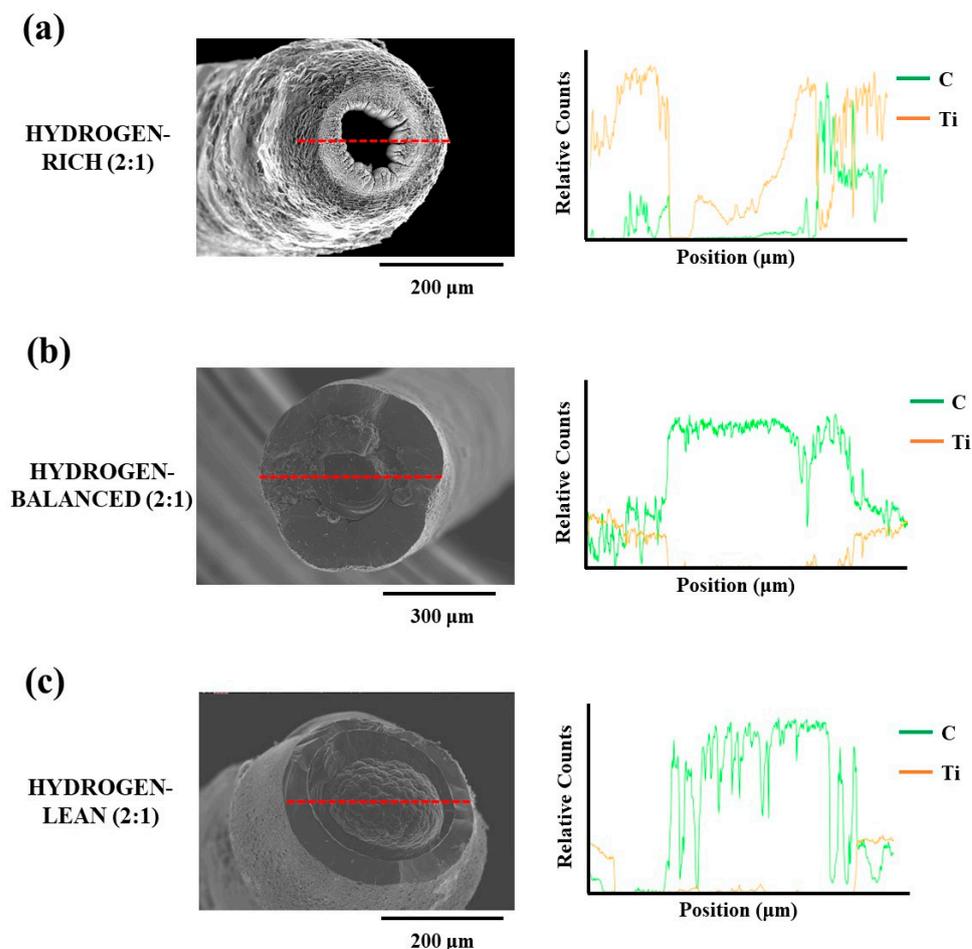
HYDROGEN-
LEAN (2:1)

Figure 5. Line profiles (shown by the red line) with corresponding XEDS data for the (**a**) Hydrogen-rich (2:1) (**b**) Hydrogen-balanced (2:1) and (**c**) Hydrogen-lean (2:1) deposits.

In Figure 5b,c the core region of these fibers have a carbon-rich deposit which was indexed as graphite in the XRD diffractograms and confirmed by the accompanying XEDS line profiles in Figure 5b,c. The formation of a carbon-rich core was, again, attributed to the Soret effect. With the reduced hydrogen concentration, ethylene, being the next lightest molecule for the precursors, collected itself into the warmer regions of the reaction zone and deposited as carbon under the laser focus. As the hydrogen concentration was further decreased, the carbon core grew larger for the hydrogen-lean (2:1) condition, as compared to the hydrogen-balanced (2:1) condition, i.e., compare Figure 5c vs. Figure 5b. This would support the prior postulation that excess hydrogen in the presence of ethylene formed hydrocarbons that became more difficult to reduce thereby resulting in a smaller carbon core for the higher hydrogen concentrated mixture. In addition, the morphology of this carbon core in the hydrogen-lean (2:1) fiber had a nodular appearance whereas the hydrogen-balanced (2:1) fiber's carbon core had a smooth surface. The formation of a nodular structure seen in the hydrogen-lean (2:1) fiber's carbon core is characteristic of growth in the mass transport limited regime whereas a smooth surface is noted in surface kinetic limited growth [25]. The mass transport limited region occurs when the growth rate is sufficient such that a boundary layer forms around the reaction zone causing all subsequent growth to be diffusion controlled through this boundary layer [24,27].

In terms of fiber diameters, Table 2 tabulates that all three hydrogen mixtures for the 2:1 ratio yielded diameters from approximately 300 to 600 μm. As the Gaussian laser beam profile is approximately 65 μm, which is significantly smaller than the deposited fiber diameter, this difference in size is contributed to the heat zone created around the deposition. The reaction of Ti and C is exothermic. The associated heat that would be

released from their reaction together provided additional warming around the reaction zone to increase the radial deposition. This coupled with a slow growth rate gave extended time for the TiC deposition allowing the fiber diameter to be larger than that of the laser beam profile itself. Note that there was a modest increase in diameter with a decrease in hydrogen content. By reducing the high thermal conductivity hydrogen gas from the reaction, this would allow heat to remain in the reaction zone that could explain this modest change in fiber diameter. In other words, as hydrogen was reduced in concentration, it became less effective in assisting in the dissipation of heat and, by default, a higher temperature promoted the TiC deposition. This would explain the increasing diameter trend with the decreasing hydrogen mixture content in Table 2.

Figure 6 plots the calculated intrinsic growth rate for each concentration for up to ten fibers sequentially, when possible. For the hydrogen-rich (2:1) condition, only three fibers are plotted because of the aforementioned stunted growth, Figure 3a. As could be expected based on the rational for the stunted growth (loss of hydrogen as a reducing agent with each deposition), the intrinsic growth rate decreased with each sequential fiber in this mixture. In the hydrogen-balanced (2:1) condition, the growth rates showed a variation from approximately 44 μm/s to as low as 30 μm/s, highlighting the complexity to retain a consistent growth speed at this mixture in this sealed batch process. In the hydrogen-lean (2:1) condition, the growth rate was much more invariant with a rate near 40 μm/s. This growth rate stabilization is contributed to GPN since not all the carbon is fully contributing to the fiber growth allowing it to grow at one particular rate as the carbon is also nucleating throughout the chamber. In addition, the reduced hydrogen also impacted the reduction in the titanium halide, which then limits the amount of titanium available to outgrow the carbon deposition. Any further reduction in hydrogen would not result in faster growth rates but instead would just increase the rate of carbon nucleation in the chamber and/or diminish the reduction in the titanium precursor. While such a hydrogen-lean (2:1) condition may yield a more stable growth rate, the formation of carbon soot clouds the viewing ports in the chamber, as well as coats the fiber deposits, Figure 2c, which are all detrimental. Thus, this growth condition and gas mixture is not an optimal setting to operate within, even though stability in the fiber growth can be achieved.

Recognizing that the hydrogen-balanced (2:1) condition yielded a consistent TiC fiber, as seen in Figure 3b, this hydrogen condition was maintained, but now the C_2H_4:$TiCl_4$ ratio was balanced as one-to-one. Here, these fibers are referred to as the hydrogen-balanced (1:1) condition, which consisted of a percent pressure of 50% H_2, 25% C_2H_4, and 25% $TiCl_4$. Figure 7a was the time-lapsed images of this fiber growth, along with the XRD diffractogram shown in Figure 7b confirming the TiC phase. As with the hydrogen-balanced (2:1) fiber, a modest graphite peak was detected in the hydrogen-balanced (1:1) condition, but it was relatively lower in intensity via a relative comparison of the graphite to the TiC peaks in each self-contained diffractogram. This suggests that the carbon-rich core has a reduced volume fraction (or size) to TiC. Figure 7c is a representative SEM micrograph of this hydrogen-balanced (1:1) fiber, where the carbon-rich core has indeed been radially reduced in size to the hydrogen-balanced (2:1) condition, i.e., compare Figure 7c to Figure 5b,c. This reduction follows the trends associated with the Soret effect, where less ethylene concentration was available to 'crowd out' the heavier titanium halide in the warmer regions of the reaction zone that would reside under the laser focal point. Consequently, TiC became more of a phase fraction within the fiber. In addition, the hydrogen-balanced (1:1) fibers have a sizably larger diameter—680 $\pm$ 50 μm—than all other prior deposits tabulated in Table 2. While the hydrogen concentration was fixed, the relative ratio increase of the titanium halide allowed for more hydrogen to be consumed as a reducing agent, which then allowed more of the metal to react with the carbon source.
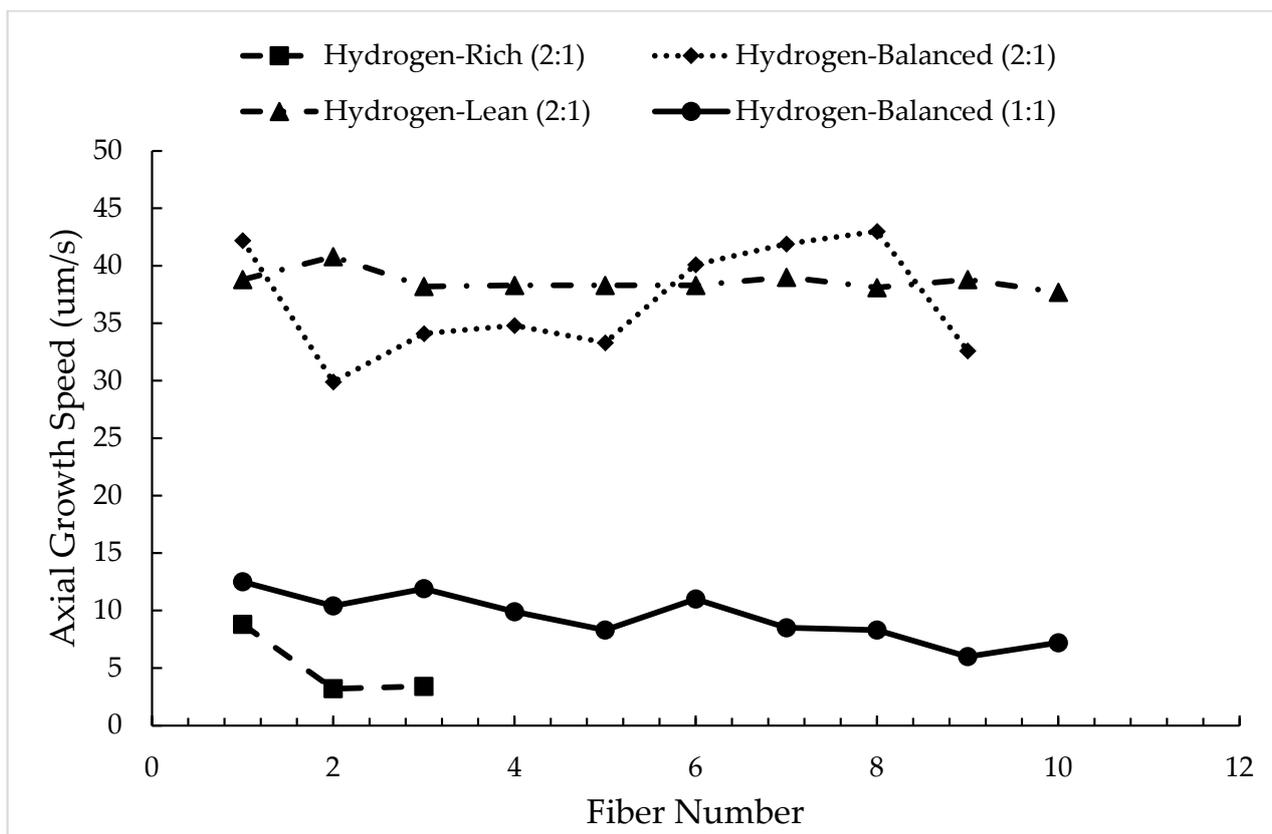
Figure 6. Growth rate as the number of sequential fibers for various precursor mixtures.
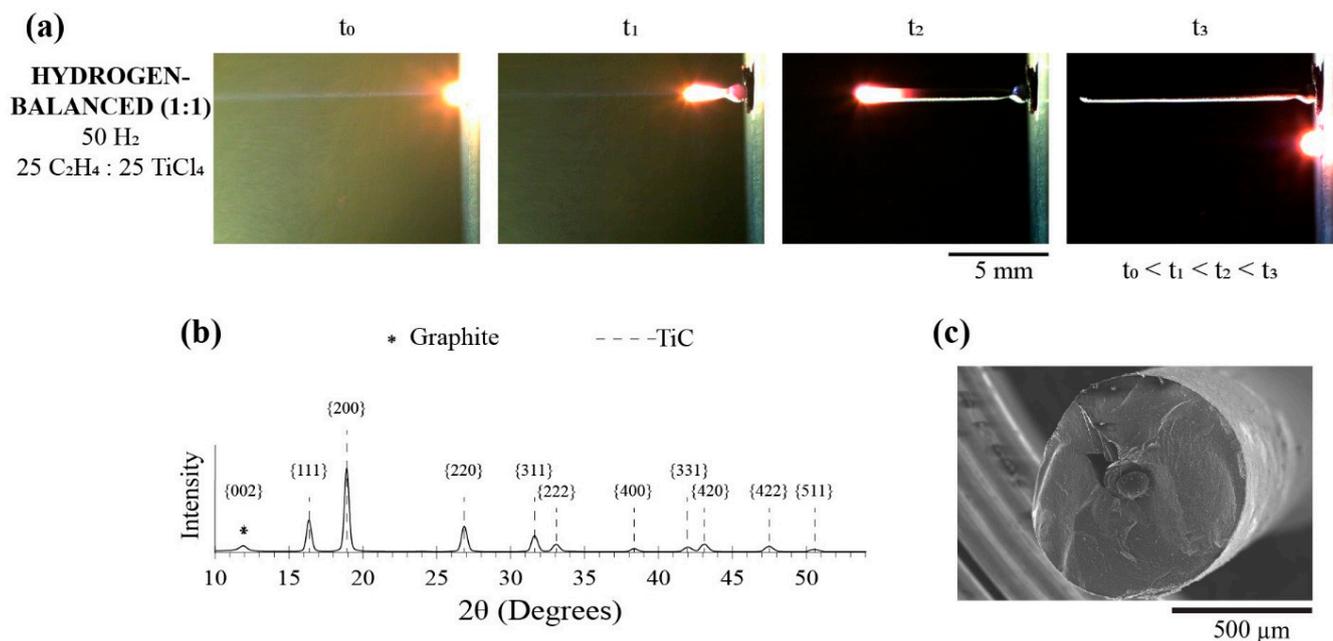

Figure 7. (**a**) Time-lapse images of the growth progression, (**b**) XRD and (**c**) SEM image of the hydrogen-balanced (1:1) condition fiber.

Figure 8 is the digital image comparison between the two-hydrogen balanced mixtures (2:1 vs. 1:1). In the hydrogen-balanced (1:1) condition, the fibers have a bronze tint, which was not apparent in the hydrogen-rich (2:1) condition. While both fibers index TiC, in their respective diffractograms, it is postulated that the bronze coloration is either from

deposited soot or a surface oxide formation. Brown carbon is a known byproduct from carbon-based fuel combustion that could occur along with black carbon at a lower rate of formation [33]. Clearly, the breakdown of ethylene, along with the heat produced during growth certainly provides the means for brown carbon to be present, especially during the hydrogen-lean (2:1) deposition where less hydrogen would be available to interact to form other types of hydrocarbons. However, the lack of gas phase nucleation in either the hydrogen-rich (2:1) or hydrogen-balanced (2:1 or 1:1) mixtures made the brown carbon less probable for the coloration. The more likely source for this coloration is a surface oxide.
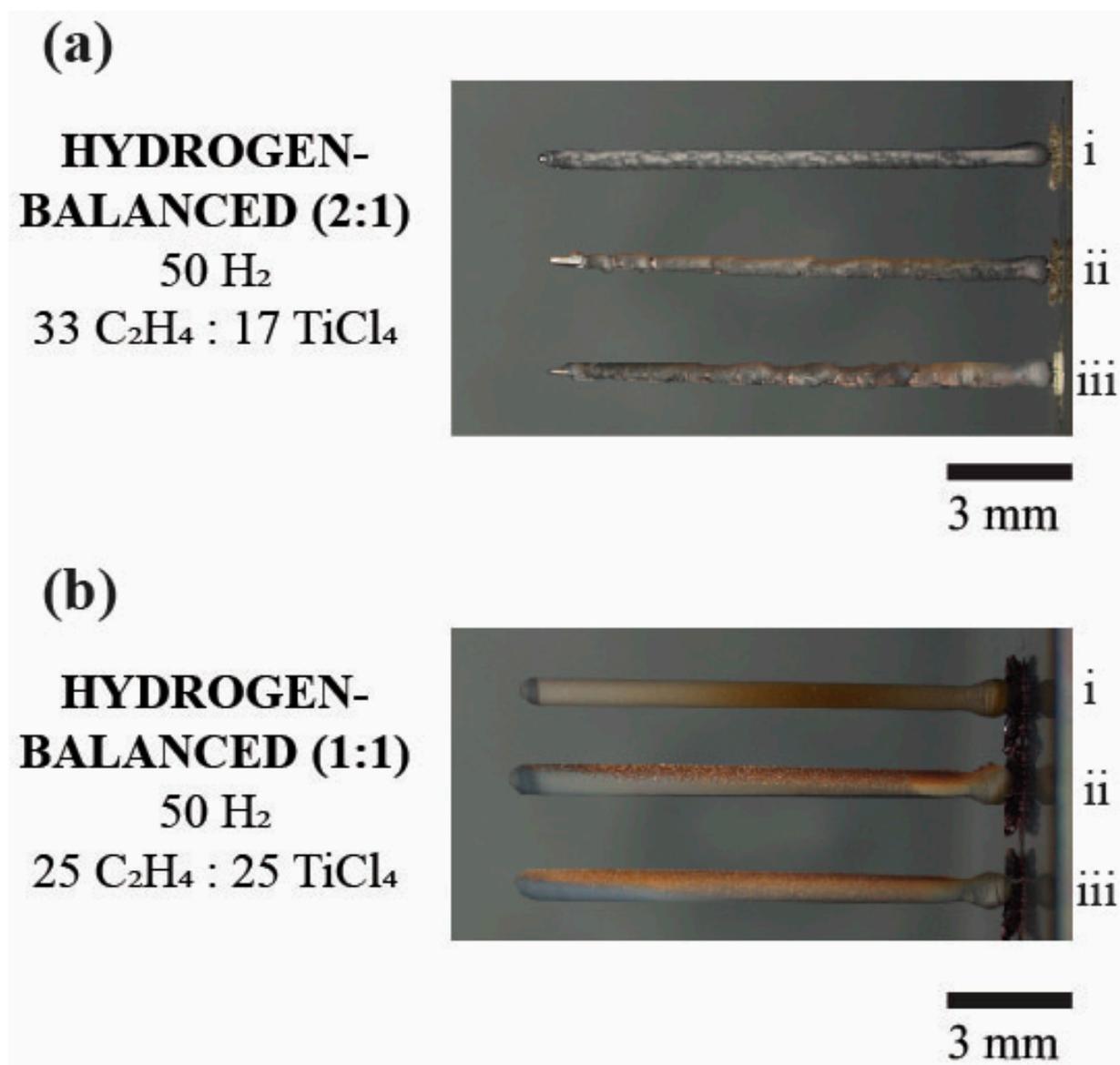
Figure 8. The digital image comparing the two hydrogen-balanced mixtures. (**a**) The hydrogen-balanced (2:1) deposit of three fibers. (**b**) The hydrogen-balanced (1:1) deposit of three fibers. Note the bronze color for the (1:1) condition vs. the (2:1) condition. The numerals i, ii, and iii denote the sequence of the fiber growth.

Titanium oxide is known to exhibit a bronze color at low temperatures and a white color at higher temperatures [34]. The hydrogen-balanced (1:1) fibers exhibited a varying temperature gradient as it deposited, which was visible in Figure 7a, and where such thermal gradients would have created convective motion of the gases around the fiber that would lead to the oxidization of titanium. As these colors were not present in the hydrogen-

balanced (2:1) condition, this mixture would have less available reduced titanium to react with any partial oxygen pressure that remained in the chamber after evacuation. While the XRD scan does not diffract the titania phase for either hydrogen-balanced mixtures, this simply indicates that titanium oxide is a minimal phase fraction and/or, more likely, a surface oxide scale. Since more titanium is being reduced in the 1:1 condition coupled with less available carbon, along with titanium's high affinity for oxygen, these fibers were more likely sensitive to the partial pressure of oxygen that was in the evacuated chamber.

Finally, the axial growth rate of the hydrogen-balanced (1:1) fibers are compared to the hydrogen-balanced (2:1) fibers plotted in Figure 6. As seen in Figure 6, the intrinsic growth rate dramatically decreases when the ethylene and titanium tetrachloride precursors are equally balanced. This reduction in speed is attributed to the increased reactivity of titanium with the carbon source, resulting in the fiber diameter increasing between these two conditions, as tabulated in Table 2. Consequently, this mixture change, even in the hydrogen-balanced condition, impacts the rate of axial growth. While the growth rate decreases, the fiber-to-fiber growth rate variation did reduce, albeit a modest decrease in rate as one sequentially grows each fiber in this sealed batch process.

4. Conclusions

In this work, the variations in gas mixture for the sequential growth of TiC fibers in a two-bar LCVD process was presented and discussed. These fibers include a hydrogen-rich, hydrogen-balanced, and hydrogen-lean mixture with respect to the sum of either a 2 C_2H_4:1 $TiCl_4$ or 1 C_2H_4:1 $TiCl_4$ precursor mixture. The presence of hydrogen is shown to be effective as a reducing agent for the titanium halide, a gas for heat transfer, a contributor towards hydrocarbon evolution, and an influencer in the fiber morphology through the Soret effect. In the hydrogen-rich regime, this results in counterproductive hydrocarbon reactions increasing the difficulty for sequential TiC fiber depositions. In the other extreme, a hydrogen-lean condition result is in gas phase nucleation whereupon carbon soot deposits itself onto prior grown fibers. For the hydrogen-balanced condition, the 2:1 mixture has relatively similar fibers deposited in terms of fiber diameter and color, but exhibits varied intrinsic growth rates between each sequentially deposited fiber suggesting some instability in the deposition process. When the ethylene and titanium halide were balanced, i.e., 1:1, for the hydrogen-balanced condition, the fibers exhibit less fiber-to-fiber growth rate variation, but their growth rates are reduced by an approximate factor of 4x to the hydrogen-balanced (2:1) condition. Furthermore, in the hydrogen-balanced (1:1) condition, the carbon-rich core that formed from the Soret effect is reduced as compared to the other (2:1) mixtures, which highlights how precursor gas chemistry controls the TiC fiber structure and morphology.

Author Contributions: Conceptualization, K.J.M. and G.B.T.; methodology, K.J.M. and G.B.T.; validation, K.J.M.; formal analysis, K.J.M. and G.B.T.; investigation, K.J.M.; resources, G.B.T.; data curation, K.J.M.; writing—original draft preparation, K.J.M.; writing—review and editing, G.B.T.; visualization, K.J.M.; supervision, G.B.T.; project administration, G.B.T.; funding acquisition, G.B.T. All authors have read and agreed to the published version of the manuscript.

Conflicts of Interest: The authors declare no conflicts of interest.

References

1. Wuchina, E.; Opila, E.; Opeka, M.; Fahrenholtz, B.; Talmy, I. UHTCs: Ultra-High Temperature Ceramic Materials for Extreme Environment Applications. *Electrochem. Soc.* **2007**, *16*, 30–36. [CrossRef]
2. Paul, A.; Binner, J.; Vaidhyanathan, B. UHTC Composites for Hypersonic Applications. In *Ultra-High Temperature Ceramics: Materials for Extreme Environment Applications*; John Wiley & Sons: Hoboken, NJ, USA, 2014; pp. 144–166.

3.　Tang, S.; Hu, C. Design, Preparation, and Properties of Carbon Fiber Reinforced Ultra-High Temperature Ceramic Composites for Aerospace Applications: A Review. *J. Mater. Sci. Technol.* **2017**, *33*, 117–130. [CrossRef]

4.　Opeka, M.; Talmy, I.; Zaykoski, J. Oxidation-based materials selection for 2000 °C + hypersonic aerosurfaces: Theoretical considerations and historical experience. *J. Mater. Sci.* **2004**, *39*, 5887–5904. [CrossRef]

5.　Chen, S.; Zeng, Y.; Xiong, X.; Lun, H.; Ye, Z.; Jiang, T.; Yang, L.; Zhang, J.; Liu, L.; Wang, G.; et al. Static and dynamic oxidation behaviour of silicon carbide at high temperature. *J. Eur. Ceram. Soc.* **2021**, *41*, 5445–5456. [CrossRef]

6.　Peters, A.; Zhang, D.; Nagle, D.; Spicer, J. Reactive two-step additive manufacturing of ultra-high temperature carbide ceramics. *Addit. Manuf.* **2023**, *61*, 103318. [CrossRef]

7.　Zhu, P.; Hong, Y.; Liu, B.; Zou, G. The synthesis of titanium carbide-reinforced carbon nanofibers. *Nanotechnology* **2009**, *20*, 255603. [CrossRef]

8.　Yu, L.; Ji, W.; Zhang, S.; Song, Y.; Liu, H.; Wang, Z.; Liu, Q.; Wang, X. Design and preparation of continuous titanium carbide fibers via simple precursor route. *Ceram. Int.* **2020**, *46*, 25485–25492. [CrossRef]

9.　Martin, J.; Borchardt, L.; Oschatz, M.; Mondin, G.; Kaskel, S. Titanium Carbide and Carbide-Derived Carbon Composite Nanofibers by Electrospinning of Ti-Resin Precursor. *Chem. Ing. Tech.* **2013**, *85*, 1742–1748. [CrossRef]

10.　Baklanova, N.I.; Zaitsev, B.N.; Titov, A.T.; Zima, T.M. The chemistry, morphology, topography of titanium carbide modified carbon fibers. *Carbon* **2008**, *46*, 261–271. [CrossRef]

11.　Li, X.; Dong, Z.; Westwood, A.; Brown, A.; Zhang, S.; Brydson, R.; Li, N.; Rand, B. Preparation of a titanium carbide coating on carbon fibre using a molten salt method. *Carbon* **2008**, *46*, 305–309. [CrossRef]

12.　Allen, S.D. Laser chemical vapor deposition: A technique for selective area deposition. *J. Appl. Phys.* **1981**, *52*, 6501–6505. [CrossRef]

13.　Mazumder, J.; Kar, A. *Theory and Application of Laser Chemical Vapor Deposition*; Springer Science & Business Media: Berlin/Heidelberg, Germany, 2013.

14.　Fauteux, C.; Pegna, J. Radial characterization of 3D-LCVD carbon fibers by Raman spectroscopy. *Appl. Phys.* **2004**, *78*, 883–888. [CrossRef]

15.　Boman, M.; Westberg, H.; Johansson, S.; Schweitz, J.A. Helical microstructures grown by laser assisted chemical vapor deposition. In Proceedings of the IEEE Micro Electro Mechanical Systems, Travemunde, Germany, 4–7 February 1992; pp. 162–167.

16.　Noel, M.S.; Kovar, D. Laser chemical vapor deposition of TiC on tantalum. *J. Mater. Sci.* **2002**, *37*, 689–697. [CrossRef]

17.　Leyendecker, G.; Bäuerle, D.; Geittner, P.; Lydtin, H. Laser induced chemical vapor deposition of carbon. *Appl. Phys. Lett.* **1981**, *39*, 921–923. [CrossRef]

18.　Maxwell, J.L.; Boman, M.; Springer, R.W.; Narayan, J.; Gnanavelu, S. Hyperbaric Laser Chemical Vapor Deposition of Carbon Fibers from the 1-Alkenes, 1-Alkynes, and Benzene. *J. Am. Chem. Soc.* **2006**, *128*, 4405–4413. [CrossRef]

19.　Fronk, K.; Cook, C.; Thompson, G. Laser Chemical Vapor Deposition of Hierarchical TiC Fibers and Tubes. *JECS* **2024**. *under review*.

20.　Westberg, H.; Boman, M.; Carlsson, J.O. Kinetics in thermal laser-assisted chemical vapour deposition of titanium carbide. *Thin Solid Films* **1992**, *218*, 8–14. [CrossRef]

21.　Pierson, H.O.; Lieberman, M.L. The chemical vapor deposition of carbon on carbon fibers. *Carbon* **1975**, *13*, 159–166. [CrossRef]

22.　Jiang, C.C.; Goto, T.; Hirai, T. Preparation of titanium carbide plates by chemical vapour deposition. *J. Mater. Sci.* **1990**, *25*, 1086–1093. [CrossRef]

23.　Rife, J.L.; Kung, P.; Hooper, R.J.; Allen, J.; Thompson, G.B. Structural and mechanical characterization of carbon fibers grown by laser induced chemical vapor deposition at hyperbaric pressures. *Carbon* **2020**, *162*, 95–105. [CrossRef]

24.　Maxwell, J.; Krishnan, R.; Haridas, S. High pressure, convectively-enhanced laser chemical vapor deposition of titanium. In Proceedings of the 1997 International Solid Freeform Fabrication Symposium, Austin, TX, USA, 11–13 August 1997.

25.　Halstead, M.P.; Leathard, D.A.; Marshall, R.M.; Purnell, J.H. The reaction of hydrogen atoms with ethylene. *Proc. R. Soc. Lond. Math. Phys. Sci.* **1970**, *316*, 575–591.

26.　Cook, C.A.; Thompson, G.B. Characteristics of methane and ethylene on additively deposited carbon fibers. *Carbon Trends* **2023**, *11*, 100258. [CrossRef]

27.　Cook, C.A.; Thompson, G.B. Additively manufactured characteristics of carbon fibers deposited from alkane precursors. *Materialia* **2023**, *32*, 101877. [CrossRef]

28.　Luidold, S.; Antrekowitsch, H. Hydrogen as a reducing agent: Thermodynamic possibilities. *Jom* **2007**, *59*, 8–62. [CrossRef]

29.　Kempers, L.J.T.M. A comprehensive thermodynamic theory of the Soret effect in a multicomponent gas, liquid, or solid. *J. Chem. Phys.* **2001**, *115*, 6330–6341. [CrossRef]

30.　Cook, C.A.; Fronk, K.; Thompson, G.B. The Soret Effect in Laser Chemical Vapor Deposited Carbon Fibers. *Chem. Pap.* **2024**, *in press*. [CrossRef]

31.　Delhaes, P. Chemical vapor deposition and infiltration processes of carbon materials. *Carbon* **2002**, *40*, 641–657. [CrossRef]

32.　Maxwell, J.; Boman, M.; Springer, R.; Nobile, A.; DeFriend, K.; Espada, L.; Sandstrom, M.; Kommireddy, D.; Pegna, J.; Goodin, D. Process–Structure Map for Diamond-Like Carbon Fibers from Ethene at Hyperbaric Pressures. *Adv. Funct. Mater.* **2005**, *15*, 1077–1087. [CrossRef]

33. Andreae, M.O.; Gelencsér, A. Black carbon or brown carbon? The nature of light-absorbing carbonaceous aerosols. *Atmos. Chem. Phys.* **2006**, *6*, 3131–3148. [CrossRef]
34. Sim, S.R.; Ryu, D.W. A Method for Instant Estimation of the Temperature Experienced by Fire-Damaged Reinforced Concrete Structures Using Titanium. *Materials* **2020**, *13*, 1993. [CrossRef]